Regioselective access to orthogonal Diels-Alder C$_{60}$ bis-adducts and tris-heteroadducts via avant-garde supramolecular mask strategy

Míriam Pujals,[†] Tània Pèlachs,[†] Carles Fuertes-Espinosa,[†] Teodor Parella,[ξ] Marc Garcia-Borràs,*,[†] Xavi Ribas[†]*

[†] Institut de Química Computacional i Catàlisi (IQCC) and Departament de Química, Universitat de Girona, Campus de Montilivi, E-17003 Girona, Catalonia, Spain

[ξ] Servei de RMN, Facultat de Ciències, Universitat Autònoma de Barcelona, Campus UAB, Bellaterra, E-08193 Catalonia, Spain

ABSTRACT: The regioselective poly-functionalization of highly symmetric spherical I_h-C$_{60}$ is extremely challenging and usually leads to the formation of regio-isomeric mixtures not amenable for HPLC purification. Recently, we have pioneered the regioselective functionalization of C$_{60}$ fullerene under a supramolecular mask strategy, using tetragonal prismatic nanocapsules to encapsulate C$_{60}$ and performing the Bingel tetrakis-cyclopropanation at the exposed fullerene surface through the four windows of the nanocapsule. Here, we describe an extension of the supramolecular mask strategy for the selective Diels-Alder (DA) functionalization of I_h-C$_{60}$ using acenes. The supramolecular mask allows the chemo- and regioselective synthesis of e,e-bis-anthracene-C$_{60}$ (functionalization at 90°) or the synthesis of $trans$-1-bis-pentacene-C$_{60}$ (functionalization at 180°), only by changing the acene length. Moreover, the mask strategy allows to obtain unprecedented equatorial hetero-tris-functionalized-C$_{60}$ adducts combining Diels-Alder with Bingel mask regiofunctionalization. Computational modelling revealed significant differences in the host-guest interactions and equilibrium established between the firstly formed anthracene- and pentacene-based monoadducts with the nanocapsule, respectively, which finally determine the observed orthogonal regioselectivity. The combination of Molecular Dynamics (MD) simulations and analysis of Frontier Molecular Orbital (FMO) involved in the Diels-Alder cycloadditions provide crucial insights to rationalize the regioselective control exerted by the supramolecular mask.

INTRODUCTION

The controlled regioselective poly-functionalization of icosahedral isomer I_h-C$_{60}$ is a very challenging task that was clearly identified soon after the discovery of fullerenes.[1-4] Because its high symmetry, usually the functionalization of fullerenes with multiple addends lead to mixtures of nonequivalent regioisomers, and their purification using multi-step HPLC separation is tedious and usually not practicable.[5-6] Pioneers in the field designed non-chromatographic synthetic strategies in the 90's to overcome the intractable complex mixtures of regioisomers commonly obtained, mainly the tether-directed remote functionalization reported by Diederich,[7-8] or the "orthogonal transposition" synthetic method developed by Kräutler[9-10] as the mainstream strategies. However, these protocols bear important drawbacks, since a) tethers cannot be removed and are left on the fullerene derivative, unless cleavable di-$tert$-butylsilylene protecting groups within the tether are used;[11-12] and b) high temperatures are required (>180 °C) to synthetize pure poly-derivatives at the solid-state, such as the example of the synthesis of $trans$-1-bis-anthracene-C$_{60}$, which was further used as a template to obtain equatorial tetrakis-C$_{60}$-adducts by means of Bingel cyclopropanation.[9] In short, the synthesis of regioisomerically pure poly-derivatives, if attainable, is envisioned as a brake-lift opportunity for their broad applicability, allowing the incorporation of these compounds into many types of materials and devices.[6]

Recently, we have pioneered the use of supramolecular tetragonal prismatic nanocapsules with a dual purpose: a) first, to serve as high-affinity host of C$_{60}$,[13] and b) secondly, to be used as supramolecular masks for the regioselective functionalization of the trapped fullerene,[14] by exposing limited portions of its surface through the windows of the nanocapsule. Specifically, the supramolecular mask allowed the regioselective Bingel cyclopropanation of C$_{60}$ through the cross-shaped windows of the nanocapsule, while simultaneously withstanding the reaction conditions. In this manner, isomer-pure poly-adducts featuring from two to four addends along the equatorial belt were synthesized, i.e. bis-, tris- and tetrakis-adducts (Figure 1b).[14] More recently, a more sophisticated three-shell matryoshka-like complex was used to further restrict the exposed surface of the encapsulated C$_{60}$, obtaining exclusively the pure Bingel $trans$-3-bis-diethylmalonate-C$_{60}$ adduct (Figure 1c).[15] It should be noted that the highly symmetric $trans$-1 bis-adduct is electronically highly disfavored and stands as the holy gray for the C$_{60}$ bis-functionalization. In addition, Beuerle and coworkers reported in 2020 the use of a trigonal bipyramidal covalent organic cage as a shadow mask for the regioselective 1,3-dipolar Prato functionalization of trapped C$_{60}$ (Figure 1a),[16] obtaining predominantly symmetry-matched tris-adducts as mixture of 4 regioisomers (out of 46 possible). Therefore, a nanocapsule fullerene hosts of a given symmetry and a specific number of windows can a priori meet the requirements, but most importantly, the mask has to survive the necessary reaction conditions.

Herein, we report the extension of the supramolecular mask strategy to the Diels-Alder (DA) regioselective functionalization of C$_{60}$ using acenes (Figure 1d). Only by changing the length of the acene (anthracene (An) versus pentacene (Pn)), $trans$-1-bis-Pn-C$_{60}$ was obtained, in contrast to the e,e-bis-An-C$_{60}$ isomer. Moreover, the mask strategy allows to obtain equatorial hetero-tris-functionalized-C$_{60}$ adducts combining Diels-Alder with Bingel mask regiofunctionalization. Computational modelling combining Molecular Dynamics (MD) simulations and electronic structure analyses afford a clear understanding of the regioselective control achieved by the nanocapsule. Simulations demonstrated that a

different host-guest equilibrium occurs between the nanocapsule and the anthracene vs pentacene mono-adducts. The different accommodation of the respective mono-adducts in the supramolecular mask differently limits which positions are accessible for a selective Diels-Alder bis-functionalization, thus leading to a different bis-functionalization pattern.
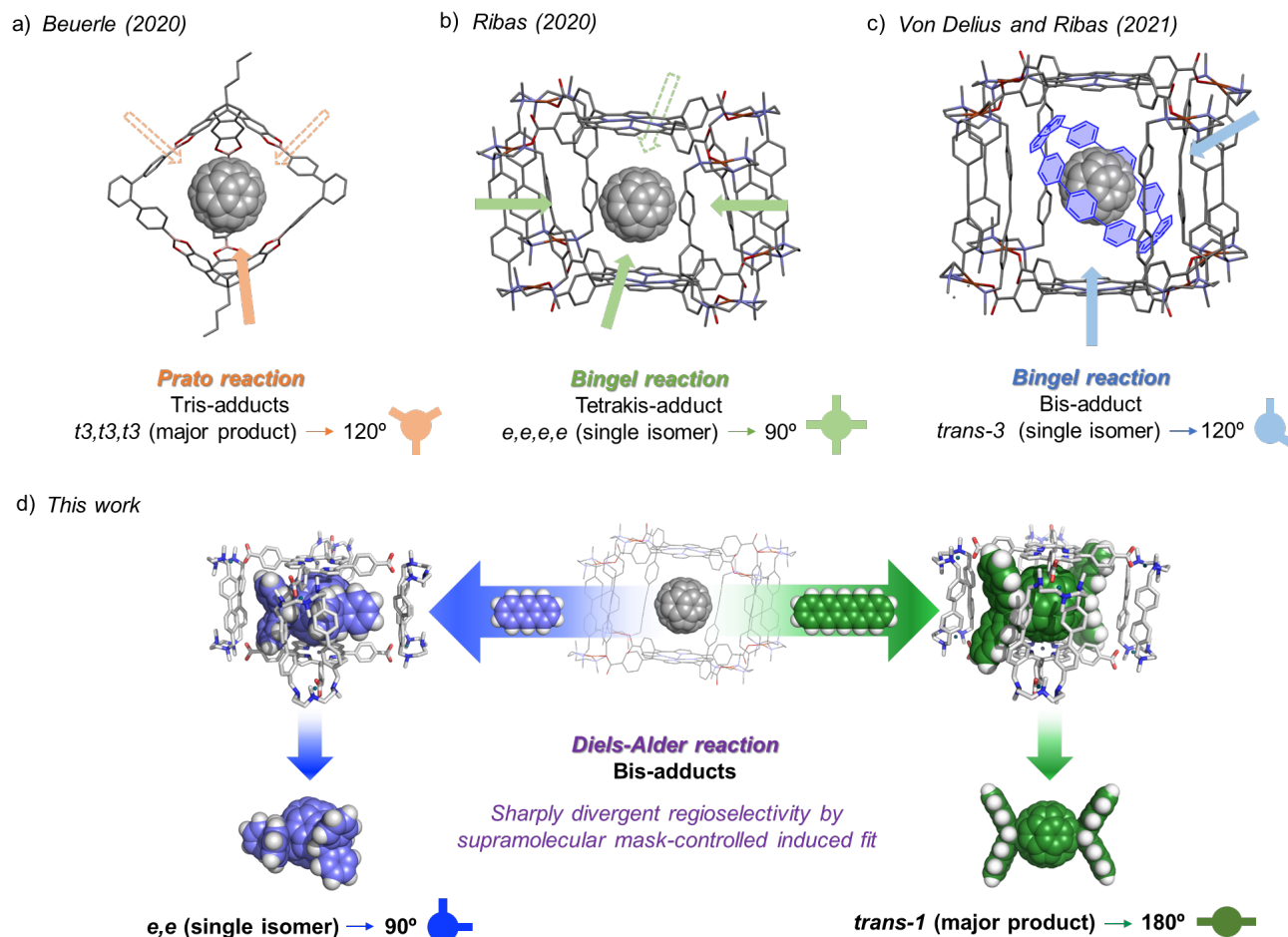

Figure 1. Strategies reported for the regioselective synthesis of C$_{60}$ poly-adducts. a) Host-guest complex featuring a trigonal bipyramidal covalent organic cage to improve the regioselectivity of Prato reaction on C$_{60}$. The *t3,t3,t3*-tris-adduct is obtained as the major product in a mixture of 4 regioisomers. b) Host-guest complex featuring a tetragonal prismatic nanocapsule to regiofunctionalize C$_{60}$ through the four cross-shaped gates of the cage. The *e,e,e,e*-tetrakis-adduct is obtained as the unique regioisomer. c) Matryoshka-like three-shell complex featuring a prismatic tetragonal cage which encapsulates an aromatic [10]cycloparaphenylene ring and, in turn, C$_{60}$ fullerene. The symmetry-mismatched *trans*-3-bis-adduct is obtained as the unique product of the reaction. d) This work: extension of the supramolecular mask strategy to Diels-Alder reactivity to obtain chemo- and regioselectively the *e,e*-bis-An-C$_{60}$ or the *trans*-1-bis-Pn-C$_{60}$ depending solely on the different host-guest equilibrium established due to the acene size.

RESULTS AND DISCUSSION

Regioselective Diels-Alder bis-functionalization of C$_{60}$ using the supramolecular mask strategy. We started the present study challenging the use of the tetragonal prismatic nanocapsules **1a**·(BArF)$_8$ (Pd^{II}-based)[13] and **1b**·(BArF)$_8$ (Cu^{II}-based)[17-18] as masks for the regioselective Diels-Alder functionalization. The mild Diels-Alder reaction conditions compared to the previously reported successful Bingel functionalization[14] were envisioned as convenient for the overall stability of the nanocapsule along the reaction course.

As expected, the reaction of C$_{60}$⊂**1a**·(BArF)$_8$ with 30 equiv. of anthracene (An) in CH$_3$CN at 50ºC for 48 hours afforded mono- and bis-adducts in a ratio 1:2.4, as monitored by HRMS (Figure 2c). Attempts to increase the ratio towards bis-adducts have been unsuccessful due to the interplay of the retro-Diels-Alder reaction (Figure S2a). The functionalized product was isolated by solvent-washing[13] with CHCl$_3$ and, remarkably, a single bis-An-C$_{60}$ isomer formed, which was isolated in 38% yield (HPLC crude also shows the presence of mono- and tris-adducts, see Figure S2b). NMR characterization clearly indicated that *e,e*-bis-An-C$_{60}$ (**2**) is formed, with a distinctive 2:1:1 pattern (rising from the C$_s$ symmetry of the product) corresponding to the cycloadded C$_{sp3}$-H signals of the anthracene addends in an equatorial fashion (Figure 2d and S4-S10, S58). This represents a very remarkable control of the regioselectivity, because previous studies showed that bare C$_{60}$ affords bis- and tris-anthracene adducts, and among the bis-adducts, a mixture of five different isomers were found (16% *ee*, 1.3% *trans*-1, 13% *trans*-2, 26% *trans*-3, 10% *trans*-4).[19]
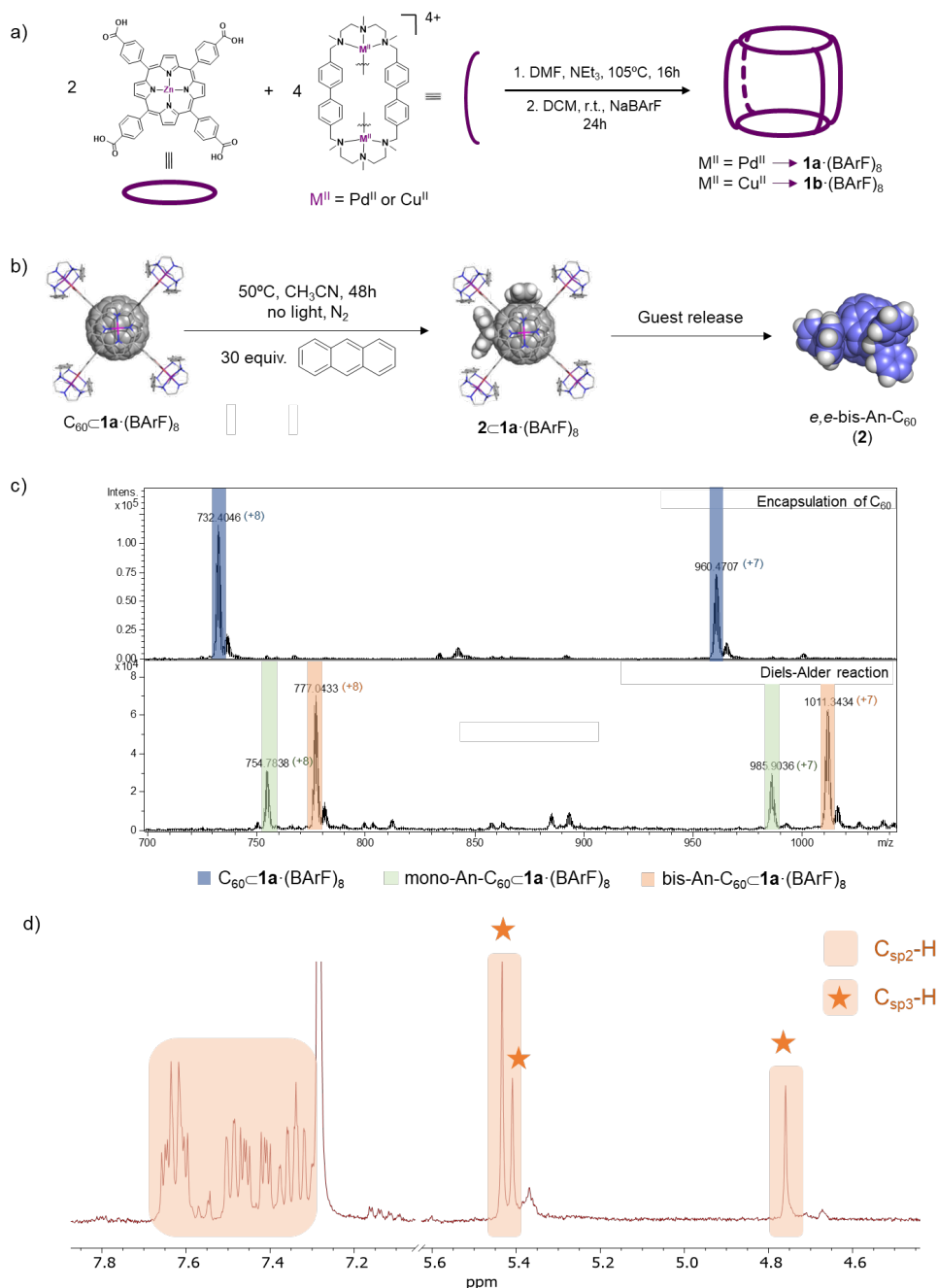
Figure 2. Synthesis and characterization of *e,e*-bis-An-C$_{60}$ (2). a) Schematic synthetic protocol of tetragonal prismatic nanocapsules **1a**·(BArF)$_8$ and **1b**·(BArF)$_8$. b) Chemo- and regioselective synthesis for **2** using **1a**·(BArF)$_8$ as supramolecular mask. c) HRMS monitoring of the synthesis of **2**⊂**1a**·(BArF)$_8$. d) ^{1}H-NMR of **2**, highlighting the cycloadded C$_{sp3}$-H of the anthracene addends.

In order to gain insight on the host-guest equilibrium established by the encapsulated mono- and *e,e*-bis-An-C$_{60}$ adducts and the nanocapsule, Molecular Dynamics (MD) simulations were performed (see computational details in SI). For each system, three replicas of MD trajectories of 1000 ns each (accumulating a total of 3 μs of simulation time) were carried out using the modelled **1a**·(Cl)$_8$ considering an explicit solvent box of acetonitrile.[14] Regarding the mono-An-C$_{60}$ system, MD simulations revealed that gate-to-gate rotation of the anthracene addend can effectively occur (Figure 4a and Figure S59a). MD simulations describe that these gate-to-gate rotations take place at the ns-μs timescale, as different rotations are observed throughout the 1000 ns of simulation time

(Figure 4a and Figure S59a). Therefore, it is expected that the anthracene moiety can explore the four symmetric gates of the capsule indistinctively, albeit longer MD trajectories would be required for the anthracene moiety to equally visit all the nanocapsule gates during the simulations (Figure S59a).

The relative orientation of the anthracene moiety respect to the porphyrin units of the capsule was also analyzed. The anthracene addend can be oriented parallel to the porphyrin moieties or perpendicular to them (Figure 4b and Figure S59b). MD simulations indicated that the interconversion between both orientations occurs fast, being the monoadduct spinning along its

C_{2v} axis, and that both orientations are indistinctively explored by the anthracene addend (Figure 4b and Figure S59b). Therefore, a highly dynamic host-guest equilibrium of the encapsulated monoadduct is described by simulations. On the contrary, MD simulations of the encapsulated e,e-bis-An-C$_{60}$ (**2**) revealed that the gate-to-gate rotation of the anthracene groups within the

nanocapsule is completely restricted and each anthracene moiety is fixed to a single gate (Figure S60). Additionally, no spinning of the bis-adduct is observed (Figure S60). This indicates that the second anthracene is responsible for restricting the rotation and dynamics of the fullerene adduct in the nanocapsule.
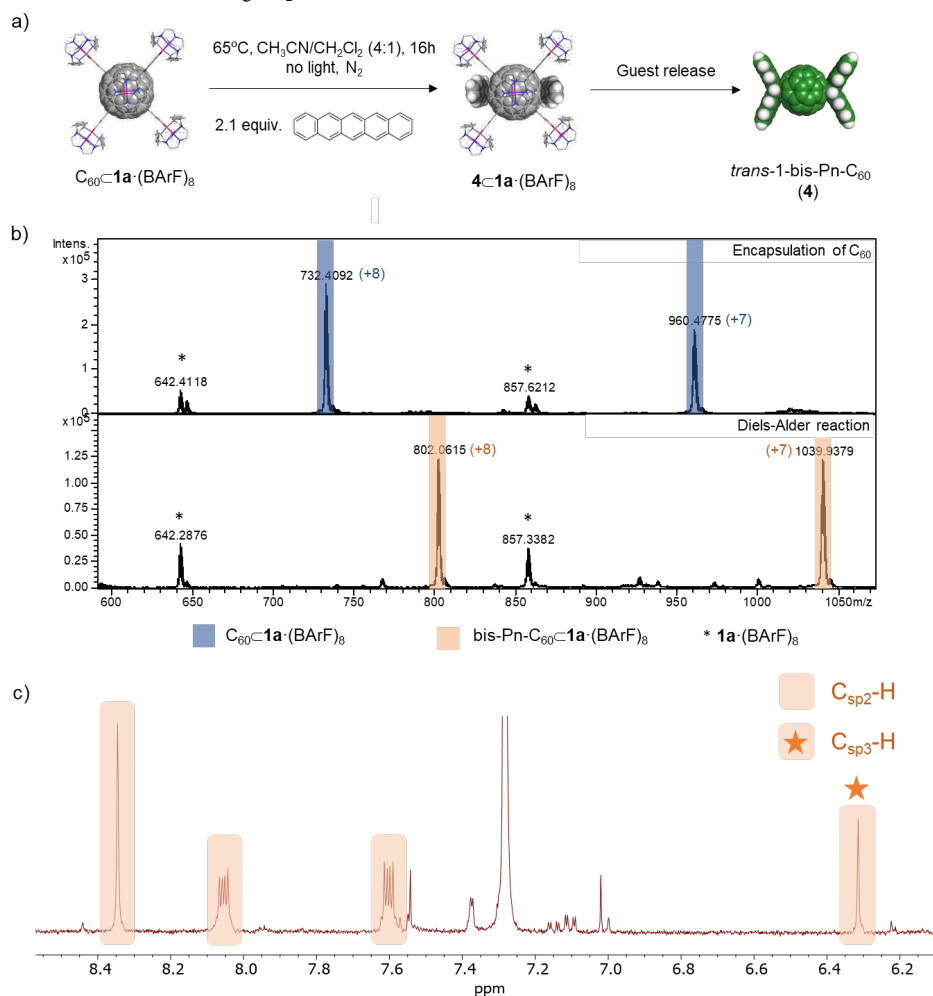

Figure 3. Synthesis and characterization for *trans*-1-bis-Pn-C$_{60}$ (4). a) Schematic representation of the synthesis for **4**. b) HRMS monitoring of the synthesis for **4**⊂**1a**·(BArF)$_8$. c) ^{1}H-NMR of **4**, highlighting the cycloadded C_{sp3}-H of the pentacene addends.

In order to understand the high regioselectivity achieved for the bis-adduct formation, the frontier molecular orbitals (FMO) involved in the Diels-Alder functionalization of the mono-An-C$_{60}$ adduct were also analyzed.[20-21] The HOMO orbital of the diene (i.e. anthracene) and the low-lying LUMOs of the dienophile (i.e. mono-adduct) were studied, while considering the geometric restrictions of the anthracene mono-adduct in the host-guest complex (Figure 5). Mono-An LUMO (-0.090 eV) has appropriate antibonding contributions on the *equatorial* bond (e bond, Figure 5.1a and 5.1b and Figure S64), while close in energy LUMO+1 (0.117 eV) has orbital antibonding lobes localized on the *equatorial-prime* bond (e' bond, Figure 5.2a and 5.2b and Figure S64). Functionalization of any of these two bonds (e and e') of the mono-adduct would lead to the same bis-adduct product by symmetry (e-e and e-e' bis-adducts are equivalent). Because of the dynamic host-guest equilibrium and the spin rotation of the mono-An characterized by MD simulations, both equatorial bonds (e and e') can be exposed to the nanocapsule open gate (Figure 5.1a and 5.2b), depending on the orientation of

the anthracene addend. Other bonds on the mono-An surface also exhibit appropriate antibonding LUMO or LUMO+1 contributions, however their functionalization is restricted due to sterics imposed by the nanocapsule. On the other hand, the *trans*-1 bond has antibonding LUMO+2 orbital contributions, and it is accessible from the opposite gate of the nanocapsule (Figure 5.3a and 5.3b and Figure S64). However, the significantly higher energy of this LUMO+2 molecular orbital (0.411 eV) respect to the LUMO and LUMO+1 makes the *trans*-1 bond much less reactive than the equatorial ones, and therefore, non-preferred. Taking together the steric control imposed by the nanocapsule, the dynamic equilibrium exhibited by the host-guest complex and the distribution of reactive mono-An FMOs, the kinetically more favourable second Diels-Alder addition is expected to be at one of the equatorial positions rather than at *trans*-1, leading to the exclusive formation of the observed equatorial e,e-bis-An-C$_{60}$ (**2**).

Regioselective orthogonal Diels-Alder bis-functionalization of C$_{60}$ combining the supramolecular mask strategy and acene length for

steric control. At this stage, we reasoned that extending the acene molecule could infer a larger steric restriction that would fix the monoadduct addend position along the vertical of nanocapsule's rectangular window (perpendicular to the porphyrins), and that it might affect the nature of the bis-adduct formed. Gratifyingly, the reaction of $C_{60} \subset$ **1a**·(BArF)$_8$ with 2.1 equiv. of pentacene (Pn) in CH_3CN/CH_2Cl_2 (4/1) at 65°C for 16 hours afforded bis-adducts as main products, as assessed by HRMS (Figure 3b). Strikingly, upon nanocapsule disassembly and workup, bis-adducts were obtained in ~80% yield, since a few tris-adducts were formed during the workup (see crude HPLC in Figure S15). By further purification through preparative TLC, only one bis-adduct isomer was isolated in 30% yield (mass losses were experimented due to insolubility issues of this bis-adduct). NMR characterization confirmed that this predominant bis-adduct was the D_{2h} *trans*-1-bis-Pn-C_{60} (**4**), with a unique distinctive singlet at 6.32 ppm corresponding to the cycloadded C_{sp3}-H of the pentacene addends in a *trans*-1 fashion (Figure 3c and S17-S18, S58). When compared to the reactivity of bare C_{60} with pentacene, mono-adduct is obtained in 59% yield alongside seven bis-pentacene adducts in a combined 13% yield and not distinguishable by ^{1}H-NMR.[22]

The striking differences in regiofunctionalization between anthracene and pentacene deserved further insight. First, MD simulations were carried out with encapsulated mono-Pn-C_{60} (**3**), to study the new host-guest complex. Simulations revealed that gate-to-gate rotation of the pentacene moiety is completely restricted, and no gate-to-gate transitions are observed along the μs timescale MD trajectories (Figure 4c and S61). In this case, the pentacene moiety remains in a single gate of the capsule throughout the simulation time, in sharp contrast to what was observed for mono-An-C_{60} where gate-to-gate rotation events are observed at this timescale. In addition, analyses of MD trajectories showed that mono-Pn-C_{60} adduct explores a single relative vertical orientation respect to the nanocapsule (Figure 4d and S61). Within this orientation, the pentacene moiety is placed perpendicular to the porphyrin units due to the steric hindrance that the molecular clips of the nanocapsule exert to the extended acene. Therefore, the bulkier pentacene addend completely fixes the mono-Pn-C_{60} adduct (**3**) in a single orientation, as opposite to the dynamic equilibrium observed for the mono-An-C_{60} host-guest system.

MD simulations with the encapsulated *trans*-1-bis-Pn-C_{60} (**4**) also showed that the guest is, as expected, fixed in a unique orientation with the pentacene addends perpendicular to the porphyrins (Figure S62).
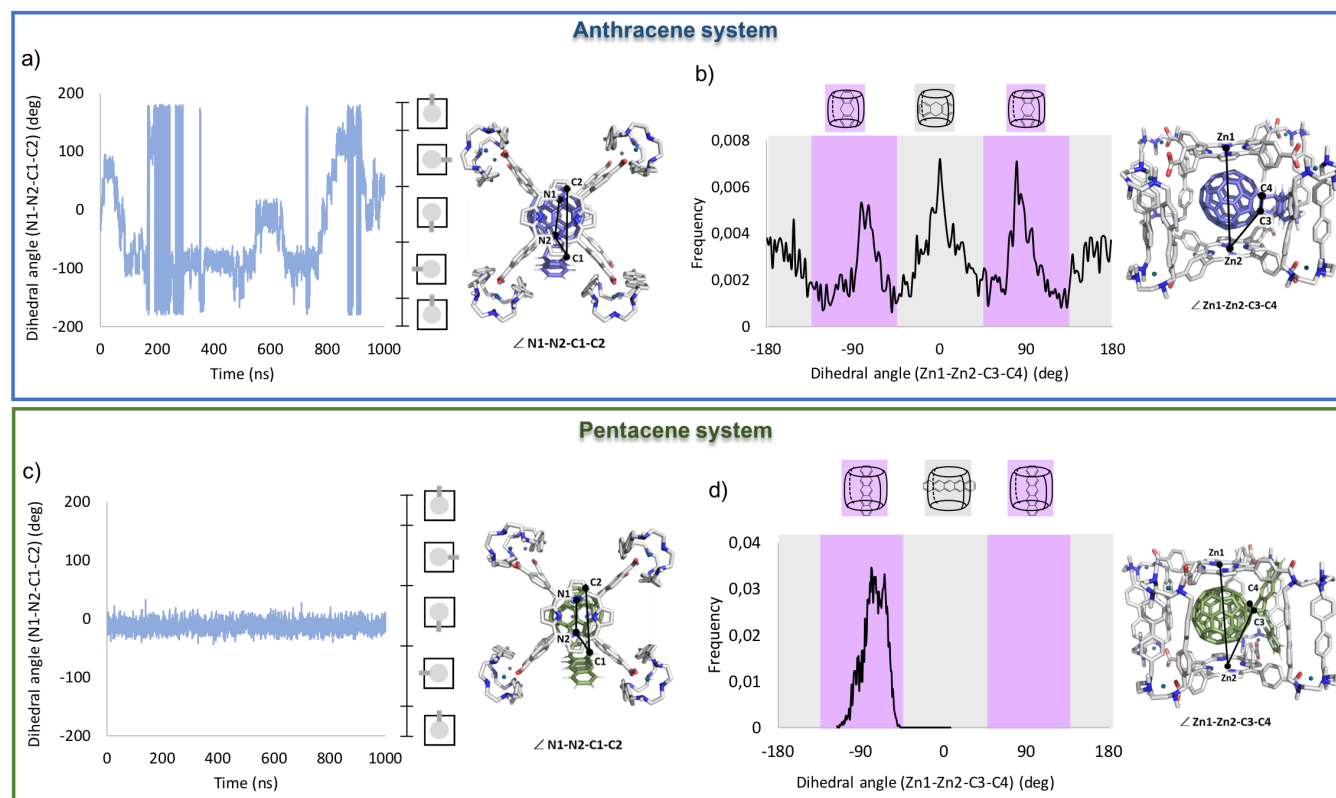

Figure 4. Analysis and characterization of the host-guest equilibria of mono-An-$C_{60} \subset$ 1a·(Cl)$_8$ and mono-Pn-$C_{60} \subset$ 1a·(Cl)$_8$ using Molecular Dynamics (MD) simulations. Analysis of anthracene mono-adduct dynamics inside the nanocage: a) ∠N1-N2-C1-C2 dihedral angle describes the relative rotation of the encapsulated mono-An-C_{60} with respect to the nanocacapsule porphyrins along the MD simulation time. N1 and N2 are atoms from the porphyrin while C1 and C2 are atoms from the fullerene derivative (see scheme). Different values explored for the ∠N1-N2-C1-C2 dihedral angle along the simulation time describe gate-to-gate rotations of the fullerene addend (see Fig. S59 for additional replicas); b) ∠Zn1-Zn2-C3-C4 dihedral angle describes the relative orientation of the fullerene acene addend with respect to the nanocapsule porphyrins. Zn1 and Zn2 are atoms from the porphyrins while C3 and C4 are atoms from the fullerene derivative (see scheme). The presented histogram plot (180 bins of 2 deg. each) describes the most visited ∠Zn1-Zn2-C3-C4 dihedral values during the 1,000 ns MD trajectory. Different values explored by ∠Zn1-Zn2-C3-C4 dihedral angle along the MD trajectory show that the anthracene addend can be equally oriented parallel or perpendicular to the nanocapsule porphyrins, being the mono-An-C_{60} spinning along its C_{2v} axis (see Fig. S61 for additional replicas). Equivalent analysis for pentacene mono-adduct dynamics inside the nanocage (mono-Pn-$C_{60} \subset$ 1a·(Cl)$_8$ system) are reported in c) and d), respectively.

To rationalize the impact that the restricted dynamism of the encapsulated pentacene mono-Pn-C$_{60}$ (**3**) has on the second DA functionalization, reactive FMOs were also analyzed considering the geometrical restrictions imposed by the encapsulation similarly to the anthracene case (see discussions above).

Within the single orientation that mono-Pn explores when formed inside the nanocapsule, with the pentacene unit vertically aligned (pointing perpendicular to the porphyrins), the first LUMO orbital (-0.095 eV) does not has antibonding contributions localized on any bond that is easily accessible from the nanocapsule open gates (Figure 5.1c and S67). Low-lying LUMO+1 (0.114 eV) has appropriate antibonding lobes on the *equatorial-prime* bond (*e'* bond) that could lead to an effective DA reaction with pentacene HOMO (Figure 5.2c and S67). Nevertheless, *e'*-bond of the encapsulated mono-Pn is oriented perpendicular to the porphyrins which imply that the second pentacene unit should approach parallel to the porphyrins (horizontally aligned) for reacting. However, due to the larger size of the pentacene and its clashing with the molecular clips, this reactive approach for functionalizing *e'*-bond in

encapsulated mono-Pn would be highly disfavored. Hence, mono-Pn should then preferentially react through the less reactive LUMO+2 orbital (0.408 eV) that has appropriate antibonding lobes localized on the *trans-1*-bond (Figure 5.3c and S67), which is oriented parallel to the porphyrins. This relative orientation of the *trans-1*-bond makes it suitable for effectively react with the bulkier pentacene, that can easily approach to this reactive bond in a vertical alignment, parallel to the porphyrins, without any steric hindrance.

Therefore, although LUMO+2 orbital with appropriate contributions on *trans-1*-bond for DA reaction is expected to be kinetically less reactive than LUMO or LUMO+1, geometric restrictions imposed by the supramolecular mask favor the regioselective formation of the *trans-1*-bis-Pn-C$_{60}$⊂**1a**·(Cl)$_8$ product. Thus, the orthogonal regiofunctionalization of C$_{60}$ to either form the *trans-1*-bisadduct with pentacene, or the equatorial *e,e*-bisadduct with anthracene, is solely driven by the different host-guest equilibrium reached by the mono-adducts that depends on the accommodation of the acene addend within the supramolecular mask.
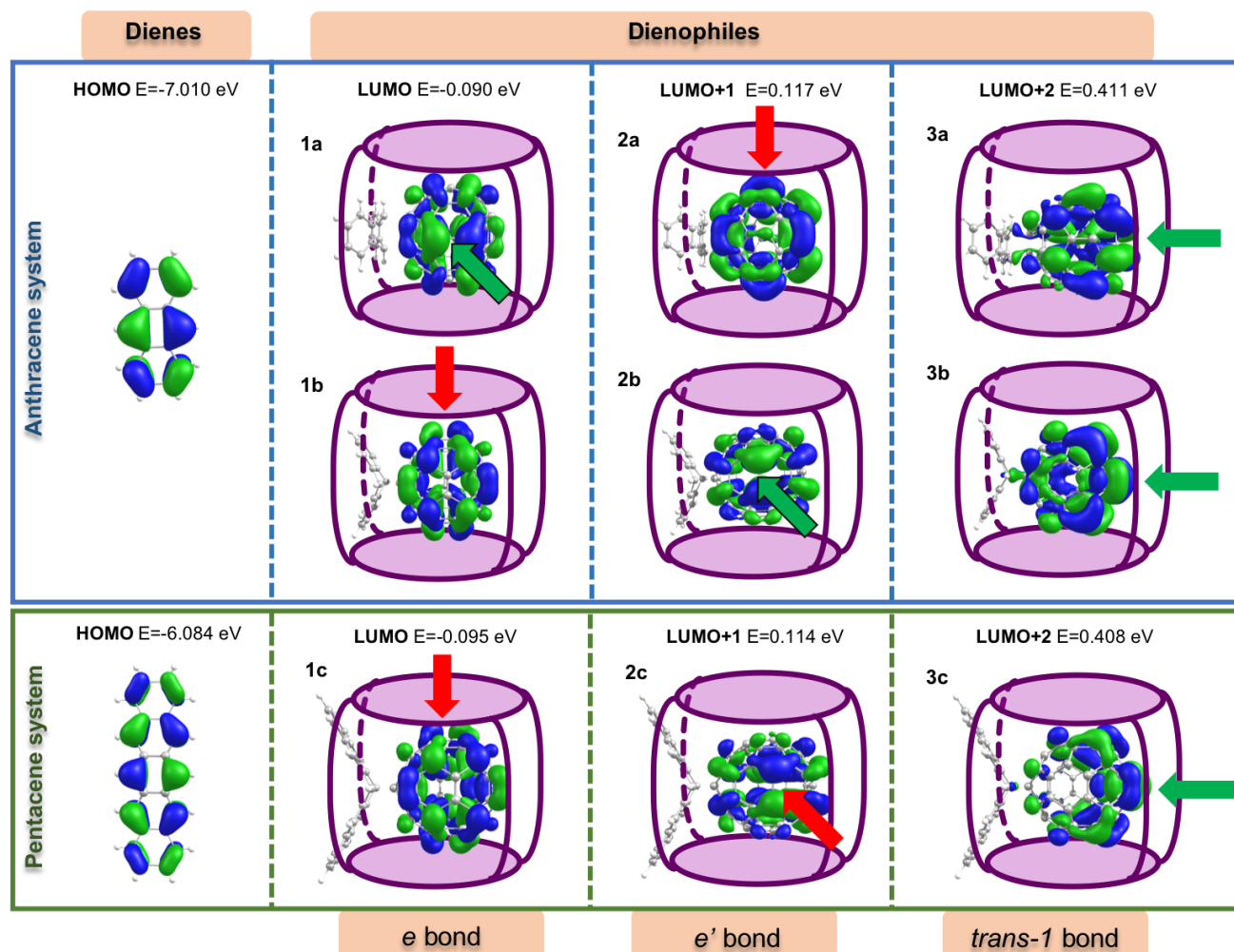

Figure 5. Frontier Molecular Orbitals (FMOs) involved in the Diels-Alder cycloadditions. HOMOs of the acenes (anthracene and pentacene) and low-lying LUMOs of the corresponding mono-adducts are reported (HF/6-31G(d,p), energies given in eV, see SI for computational details). A schematic representation of the mono-adducts' LUMOs when encapsulated is shown. For the anthracene system, two possible orientations of the mono-adduct are depicted inside the nanocapsule, considering its possible rotation as characterized from MD simulations (Fig. 4b): anthracene addend oriented parallel (1a, 2a and 3a) or perpendicular (1b, 2b and 3b) with respect to the porphyrins. For the pentacene system, only one orientation of the mono-adduct is depicted inside the nanocapsule, since its rotation is limited due of steric hindrance as observed from MD simulations (Fig. 4d and Fig. S63a): pentacene moiety oriented perpendicular with respect to the porphyrins (1c, 2c and 3c).

Controlled regioselective hetero-poly-functionalization of C₆₀. With the orthogonal *e,e*-bis-An-C₆₀ (**2**) and *trans*-1-bis-Pn-C₆₀ (**4**) as pure bis-adducts in hand, our new target was to submit them to Bingel cyclopropanation conditions under the supramolecular mask strategy, seeking the synthesis of pure-isomer hetero-poly-adducts. We rapidly noticed that re-encapsulation of **2** in the Pd[II]-based **1a**·(BArF)₈ was not efficient due to the rigidity of the gate entrances, thus we resorted to the analogous more adaptable Cu[II]-based nanocapsule **1b**·(BArF)₈,[17-18] which showed practically full encapsulation of the guest. We first focused our efforts in heterofunctionalizing the encapsulated *e,e*-bis-An-C₆₀ (**2**) by reacting it with diethyl bromomalonate and NaH (Figure 6a).[14] HRMS monitoring showed that the expected equatorial hetero-

tetrakis-adduct was formed, but in very small amount. Contrarily, a tris-adduct, i.e. *e,e*-bis-An-*e*-mono-diethylmalonate-C₆₀ (**5**), was the major product (Figure 6b). It was released from the nanocapsule by solvent-washing with CHCl₃ and, after careful NMR and UV-vis spectroscopic analyses (Figure 6c and Figure S21b), a mixture of two tris-regioisomers (isomers **5**(I) and **5**(II)) were characterized in a 1:3 ratio, respectively (Figure 6c). For both isomers the distribution of signals corresponding to the aliphatic C$_{sp3}$-H of the anthracene addends, a 2:1:1 ratio is expected. In the region of 4.8-4.9 ppm, two singlets are observed with a 1:3 ratio (4.89 ppm and 4.82 ppm, respectively), which are associated to the ratio of the two isomers. These upfield signals correspond to the anthracene protons, which are deshielded by the adjacent benzene ring of the other equatorial anthracene moiety.
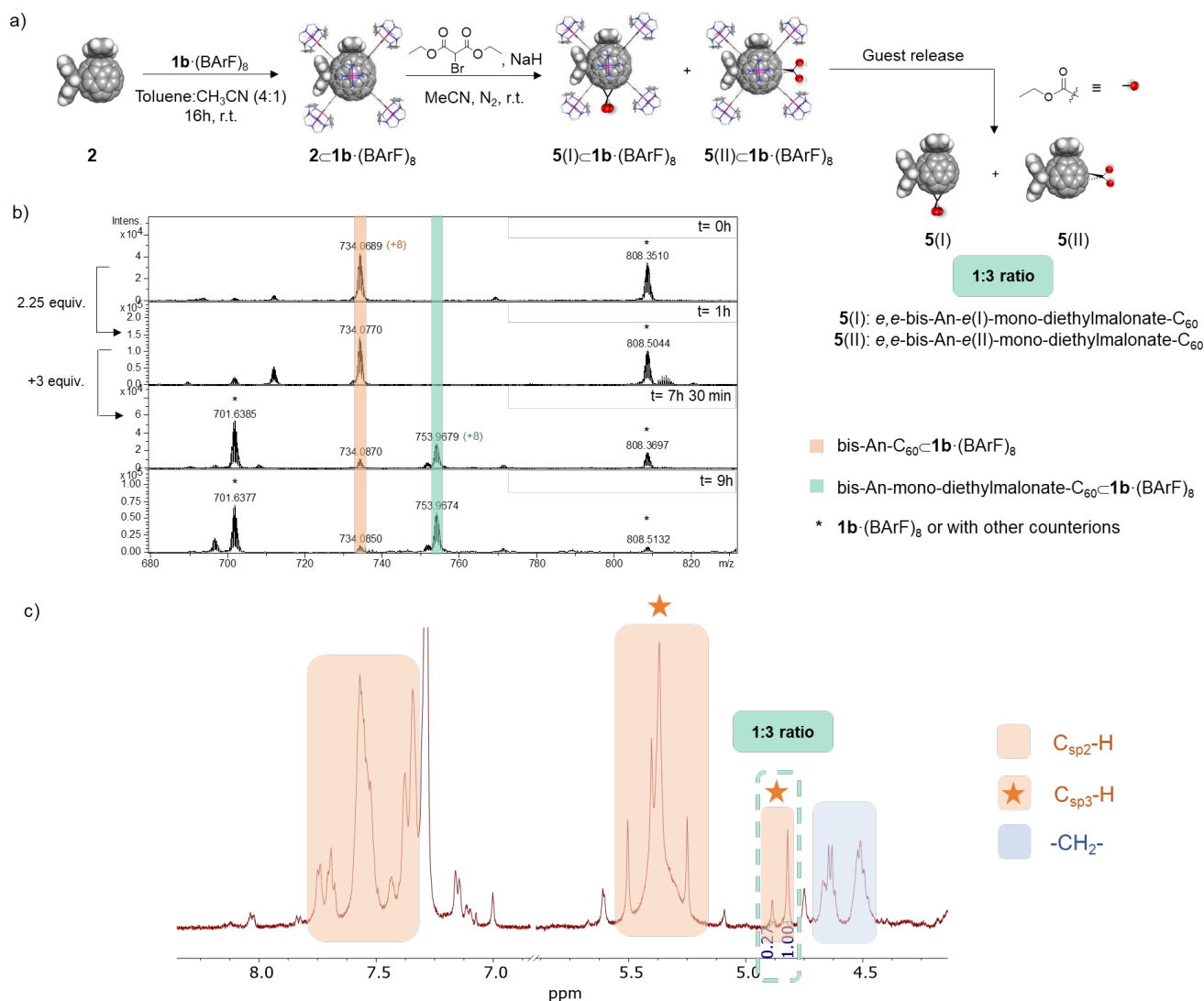

Figure 6. Synthesis and characterization for *e,e*-bis-An-*e*-mono-diethylmalonate-C₆₀ (mixture of isomers 5(I) and 5(II)). a) Schematic representation of the synthesis for **5**. b) HRMS monitoring of the synthesis for **5**⊂**1b**·(BArF)₈. c) ¹H-NMR of isomers **5**(I) and **5**(II) in a 1:3 ratio, highlighting the cycloadded C$_{sp3}$-H of the anthracene addends.

We then attempted the Bingel functionalization of *trans*-1-bis-Pn-C₆₀ (**4**). The first requisite was to perform its encapsulation, but even using the more adaptable Cu[II]-based nanocapsule **1b**·(BArF)₈, encapsulation was reached in a minimum extent, and only minor

amounts of encapsulated **4** were detected by HRMS. This was somehow expected from the computational modelling and MD analyses that described that the vertically aligned pentacene moieties perpendicular to the porphyrins stand out from the nanocage

(Figure 4d and S63b) thus sterically hindering the squeezing of the *trans*-1 compound to the nanocapsule. Therefore, we turned our focus into the Bingel cyclopropanation of encapsulated mono-Pn-C$_{60}$ (**3**), which was successfully encapsulated in **1a**·(BArF)$_8$. The heterofunctionalization was monitored by HRMS (Figure 7b), clearly showing that a tris-adduct, i.e. mono-Pn-bis-diethylmalonate-C$_{60}$, was accumulated. The equatorial hetero-tetrakis-adduct, was formed in only tiny amounts, despite pushing the experimental conditions (heating and larger reaction times). Upon releasing the product from the nanocapsule by solvent-washing, full NMR, UV-vis and MALDI-MS unambiguously led to the conclusion that *e*-mono-Pn-*trans*-1-bis-diethylmalonate-C$_{60}$ (**6**) was obtained as a unique regioisomer in a 63% yield (Figures 7, S32-S40). The singlet at 5.86 ppm in the ^{1}H NMR spectrum of **6** clearly indicates a highly symmetric *trans*-1 disposition of the cyclopropanated addends.

Once the supramolecular mask strategy for selective regiofunctionalization combining Diels-Alder and Bingel addends was demonstrated, we sought to prepare hetero-hexakis-adducts[23-24] by taking advantage of the directing ability of the Diels-Alder addends of *e,e*-bis-An-C$_{60}$ (**2**) and *trans*-1-bis-Pn-C$_{60}$ (**4**) bis-adducts. First, *e,e*-bis-An-C$_{60}$ (**2**) in solution was subjected to exhaustive Bingel cyclopropanation (40 eq. bromomalonate, 40 eq. DBU, CH$_2$Cl$_2$, r.t. 48h) to minimize the formation of hetero-tetrakis- and pentakis-adducts. In this manner, hetero-hexakis adducts (two anthracenes and four cyclopropanated addends) were mainly formed as assessed by HPLC, MALDI-MS and 2D NMR (12.5% yield) (Figure 8a, S41-S48, S58). Specifically, the 2:1:1 pattern corresponding to the cycloadded C$_{sp3}$-H signals of the anthracene addends remained intact, therefore the symmetry of the *e,e*-bis-anthracene unit suggests that the octahedral arranged *Th*-hexakis-isomer, i.e. *e,e*-bis-An-based hetero-hexakis-C$_{60}$ (**7**), is mainly obtained.
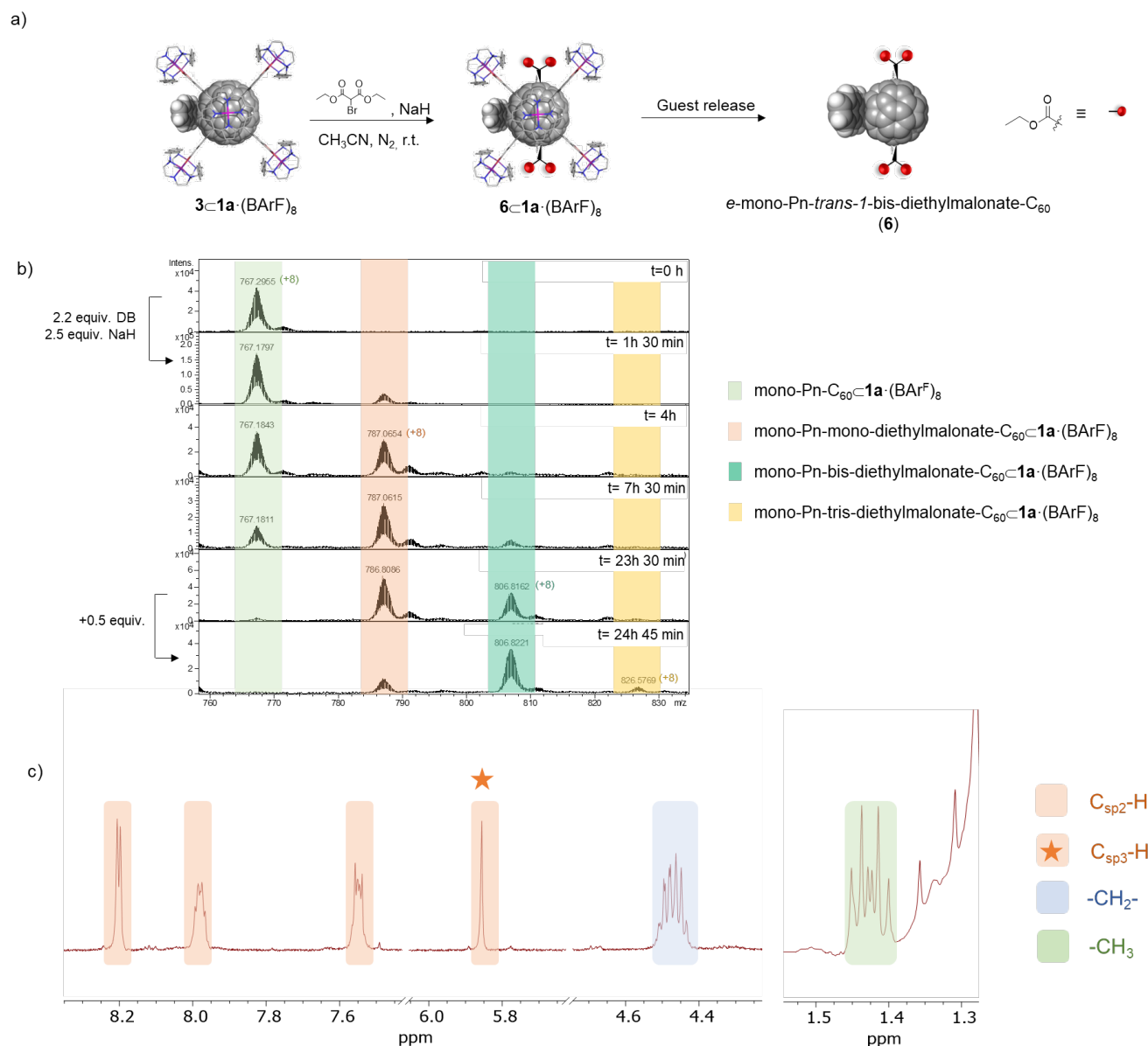

Figure 7. Synthesis and characterization for *e*-mono-Pn-*trans*-1-bis-diethylmalonate-C$_{60}$ (6). a) Schematic representation of the synthesis for **6**. b) HRMS monitoring of the synthesis for **6**⊂**1a**·(BArF)$_8$. c) ^{1}H-NMR of **6**, highlighting the singlet peak at 5.82 ppm corresponding to cycloadded C$_{sp3}$-H of the pentacene addends.

Finally, emulating Kräutler's orthogonal transposition,[9] *trans*-1-bis-Pn-C$_{60}$ (**4**) was also subjected to exhaustive Bingel cyclopropanation. The expected *Th*-hetero-hexakis-adduct (Figure 8b), i.e. *trans-1*-bis-Pn-*e,e,e,e*-tetrakis-diethylmalonate-C$_{60}$ (**8**), was formed as the unique product (MALDI-MS and 2D NMR, see Figures S49-S58) featuring all four cyclopropanated addends in the equatorial belt of the fullerene.
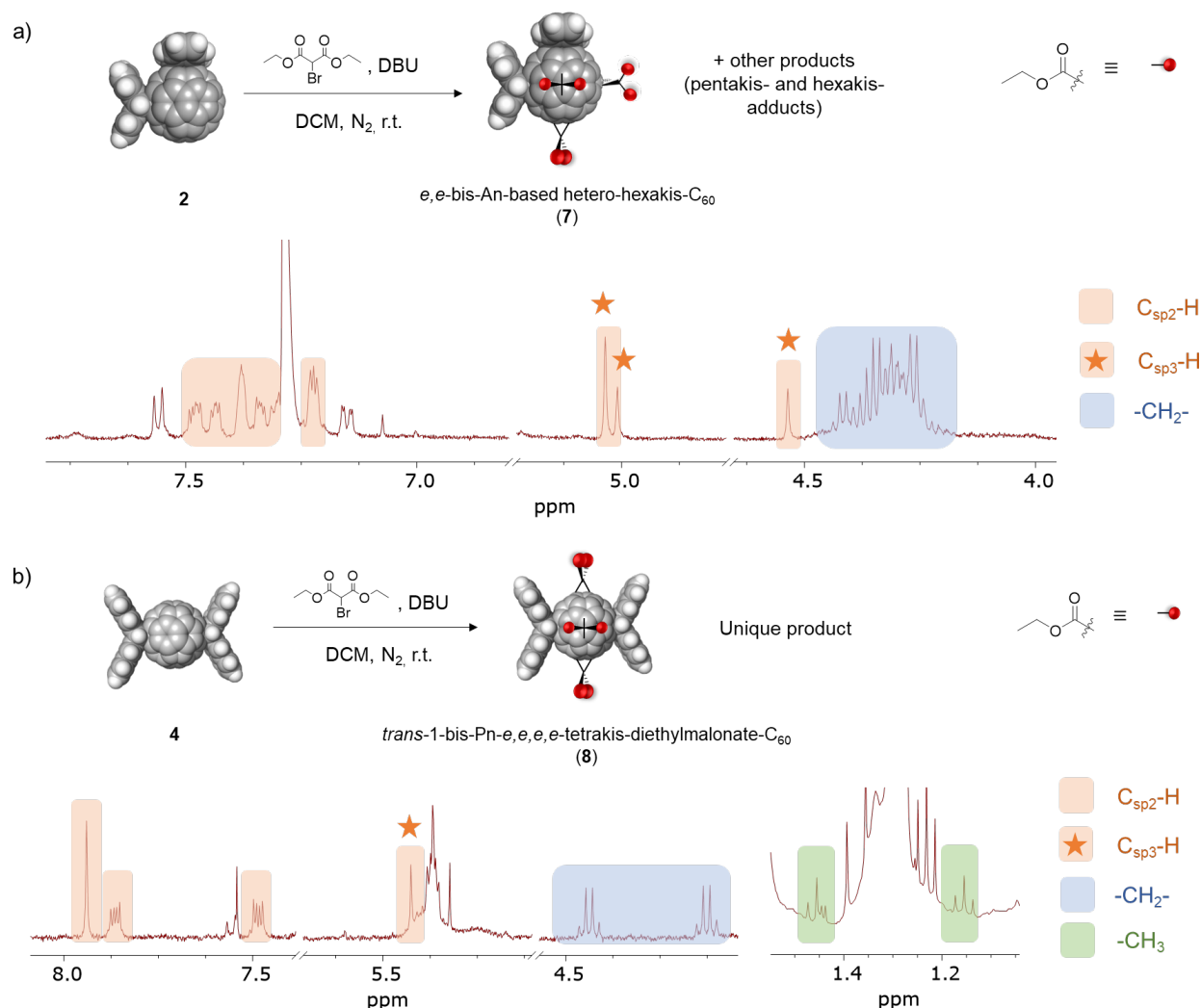

Figure 8. Synthesis and characterization for hetero-hexakis-adducts 7 and 8. a) Schematic representation of the synthesis for the *e,e*-bis-An-based *Th*-hetero-hexakis-C$_{60}$ (**7**) and the corresponding ¹H-NMR, highlighting the cycloadded C$_{sp3}$-H of the anthracene addends. b) Schematic representation of the synthesis for *trans-1*-bis-Pn-*e,e,e,e*-tetrakis-diethylmalonate-C$_{60}$ (**8**) and the corresponding ¹H-NMR, highlighting the cycloadded C$_{sp3}$-H of the pentacene addends.

CONCLUSIONS

In summary, we have demonstrated that the supramolecular mask strategy for the regiofunctionalization of C$_{60}$ can be extended to Diels-Alder cycloadditions using tetragonal prismatic nanocapsules. Moreover, the ability to orthogonally switch the regioselectivity of bis-acene-adducts from 90° (*e,e*-bis-anthracene-C$_{60}$ (**2**)) to 180° (*trans*-1-bis-pentacene-C$_{60}$ (**4**)) by simply enlarging the acene molecule is unprecedented. Computational modelling showed that the differences in the regioselectivity are induced by the different host-guest interactions established between the firstly formed anthracene- and pentacene-based monoadducts with the nanocapsule, respectively. The complementary experimental characterization and computational modelling have proved to be an ideal combination to tackle the comprehension but also for designing the orthogonal regioselectivity exhibited by these systems.

Furthermore, otherwise inaccessible Diels-Alder and Bingel poly-hetero-adducts were also obtained as equatorial tris-adducts (*e,e*-bis-An-*e*-mono-diethylmalonate-C$_{60}$ (**5**) and *e*-mono-Pn-*trans*-1-bis-diethylmalonate-C$_{60}$ (**6**)) upon submitting encapsulated bis-adduct **2** and mono-adduct **3** to Bingel cyclopropanation conditions. In this manner, we show here the validity and versatility of the supramolecular mask strategy combining different addends-type and different experimental conditions. Finally, bare *e,e*-bis-An-C$_{60}$ (**2**) and *trans*-1-bis-Pn-C$_{60}$ (**4**) were used to build molecular complexity upon them, obtaining the corresponding *Th*-hexakis isomers i.e. *e,e*-bis-An-based *Th*-hetero-hexakis-C$_{60}$ (**7**) and *trans-1*-bis-pentacene-*e,e,e,e*-tetrakis-diethylmalonate-C$_{60}$ (**8**).

This work further exemplifies that tailored supramolecular masks are a promising synthetic strategy for the development of general regioselective crafting of spheroidal fullerenes, which are not

accessible by other methodology and will find ample applications in many fields, such as photovoltaics, material science or biomedicine.

AUTHOR INFORMATION

Corresponding Author

Xavi Ribas, xavi.ribas@udg.edu
Marc Garcia-Borràs, marc.garcia@udg.edu

ASSOCIATED CONTENT

Supporting information file including all experimental methodologies employed, spectroscopic characterization of all compounds and computational details (pdf).
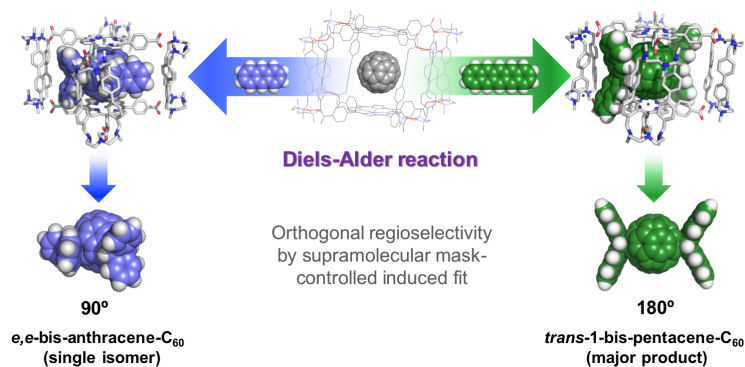
ACKNOWLEDGMENTS

REFERENCES

1. Hirsch, A.; Brettreich, M., *Fullerenes, Chemistry and Reactions*. Wiley-VCH: Weinheim, 2005.

2. Djojo, F.; Hirsch, A.; Grimme, S., The Addition Patterns of C60 Trisadducts Involving the Positional Relationships e and trans-n (n = 2–4): Isolation, Properties, and Determination of the Absolute Configuration of Tris(malonates) and Tris[bis(oxazolines)]. *Eur. J. Org. Chem.* **1999,** *1999*, 3027-3039.

3. Djojo, F.; Herzog, A.; Lamparth, I.; Hampel, F.; Hirsch, A., Regiochemistry of Twofold Additions to [6,6] Bonds in C60: Influence of the Addend-Independent Cage Distortion in 1,2-Monoadducts. *Chem. Eur. J.* **1996,** *2*, 1537-1547.

4. Hirsch, A.; Lamparth, I.; Karfunkel, H. R., Fullerene Chemistry in Three Dimensions: Isolation of Seven Regioisomeric Bisadducts and Chiral Trisadducts of C60 and Di(ethoxycarbonyl)methylene. *Angew. Chem. Int. Ed. Engl.* **1994,** *33*, 437-438.

5. Yan, W.; Seifermann, S. M.; Pierrat, P.; Brase, S., Synthesis of highly functionalized C60 fullerene derivatives and their applications in material and life sciences. *Org. Biomol. Chem.* **2015,** *13*, 25-54.

6. Fuertes-Espinosa, C.; Pujals, M.; Ribas, X., Supramolecular Purification and Regioselective Functionalization of Fullerenes and Endohedral Metallofullerenes. *Chem* **2020,** *6*, 3219-3262.

7. Isaacs, L.; Diederich, F.; Haldimann, R. F., Multiple Adducts of C60 by Tether-Directed Remote Functionalization and synthesis of soluble derivatives of new carbon allotropes Cn(60+5). *Helv. Chim. Acta* **1997,** *80*, 317-342.

8. Isaacs, L.; Haldimann, R. F.; Diederich, F., Tether-Directed Remote Functionalization of Buckminsterfullerene: Regiospecific Hexaadduct Formation. *Angew. Chem. Int. Ed. Eng.* **1994,** *33*, 2339-2342.

9. Schwenninger, R.; Müller, T.; Kräutler, B., Concise Route to Symmetric Multiadducts of [60]Fullerene: Preparation of an Equatorial Tetraadduct by Orthogonal Transposition. *J. Am. Chem. Soc.* **1997,** *119*, 9317-9318.

10. Kräutler, B.; Müller, T.; Maynollo, J.; Gruber, K.; Kratky, C.; Ochsenbein, P.; Schwarzenbach, D.; Bürgi, H.-B., A Topochemically Controlled, Regiospecific Fullerene Bisfunctionalization. *Angew. Chem. Int. Ed. Eng.* **1996,** *35*, 1204-1206.

11. Trinh, T. M. N.; Schillinger, F.; Guerra, S.; Meichsner, E.; Nierengarten, I.; Hahn, U.; Holler, M.; Nierengarten, J.-F., Regioselective Preparation of Fullerene Bis-adducts from Cleavable Macrocyclic Bis-malonates. *Eur. J. Org. Chem.* **2021,** *2021*, 3770-3786.

12. Meichsner, E.; Schillinger, F.; Trinh, T. M. N.; Guerra, S.; Hahn, U.; Nierengarten, I.; Holler, M.; Nierengarten, J.-F., Regioselective Synthesis of Fullerene Tris-adducts for the Preparation of Clickable Fullerene [3:3]-Hexa-adduct Scaffolds. *Eur. J. Org. Chem.* **2021,** *2021*, 3787-3797.

13. García-Simón, C.; Garcia-Borràs, M.; Gómez, L.; Parella, T.; Osuna, S.; Juanhuix, J.; Imaz, I.; Maspoch, D.; Costas, M.; Ribas, X., Sponge-like molecular cage for purification of fullerenes. *Nat. Commun.* **2014,** *5*, 5557.

14. Fuertes-Espinosa, C.; García-Simón, C.; Pujals, M.; Garcia-Borràs, M.; Gómez, L.; Parella, T.; Juanhuix, J.; Imaz, I.; Maspoch, D.; Costas, M.; Ribas, X., Supramolecular Fullerene Sponges as Catalytic Masks for Regioselective Functionalization of C60. *Chem* **2020,** *6*, 169-186.

15. Ubasart, E.; Borodin, O.; Fuertes-Espinosa, C.; Xu, Y.; García-Simón, C.; Gómez, L.; Juanhuix, J.; Gándara, F.; Imaz, I.; Maspoch, D.; von Delius, M.; Ribas, X., A three-shell supramolecular complex enables the symmetry-mismatched chemo- and regioselective bis-functionalization of C60. *Nat. Chem.* **2021,** *13*, 420-427.

16. Leonhardt, V.; Fimmel, S.; Krause, A.-M.; Beuerle, F., A Covalent Organic Cage Compound Acting as a Supramolecular Shadow Mask for the Regioselective Functionalization of C60. *Chem. Sci.* **2020,** *11*, 8409-8415.

17. Fuertes-Espinosa, C.; García-Simón, C.; Castro, E.; Costas, M.; Echegoyen, L.; Ribas, X., A Copper-based Supramolecular Nanocapsule that Enables Straightforward Purification of Sc3N-based Endohedral Metallofullerene Soots. *Chem. Eur. J.* **2017,** *23*, 3553-3557.

18. Fuertes-Espinosa, C.; Gómez-Torres, A.; Morales-Martínez, R.; Rodríguez-Fortea, A.; García-Simón, C.; Gándara, F.; Imaz, I.; Juanhuix, J.; Maspoch, D.; Poblet, J. M.; Echegoyen, L.; Ribas, X., Purification of Uranium-based Endohedral Metallofullerenes (EMFs) by Selective Supramolecular Encapsulation and Release. *Angew. Chem. Int. Ed.* **2018,** *57*, 11294-11299.

19. Duarte-Ruiz, A.; Müller, T.; Wurst, K.; Kräutler, B., The bis-adducts of the [5,6]-fullerene C60 and anthracene. *Tetrahedron* **2001,** *57*, 3709-3714.

20. Wang, J. Y.; Li, G.; Hao, W. J.; Jiang, B., Enantio- and Regioselective CuH-Catalyzed Conjugate Reduction of Yne-Allenones. *Org Lett* **2021,** *23*, 3828-3833.

21. Hoffmann, R.; Woodward, R. B., Selection Rules for Concerted Cycloaddition Reactions. *J. Am. Chem. Soc.* **1965,** *87*, 2046-2048.

22. Seeman, J. I., Woodward–Hoffmann's Stereochemistry of Electrocyclic Reactions: From Day 1 to the JACS Receipt Date (May 5, 1964 to November 30, 1964). *J. Org. Chem.* **2015,** *80*, 11632-11671.

23.   Mack, J.; Miller, G. P., Synthesis and Characterization of a C60-Pentacene Monoadduct. *Fullerene Sci. Tech.* **1997,** *5*, 607-614.

24.   Hirsch, A.; Vostrowsky, O., C60 Hexakisadducts with an Octahedral Addition Pattern – A New Structure Motif in Organic Chemistry. *Eur. J. Org. Chem.* **2001,** *2001*, 829-848.

25.   Hirsch, A.; Lamparth, I.; Groesser, T.; Karfunkel, H. R., Regiochemistry of Multiple Additions to the Fullerene Core: Synthesis of a Th-Symmetric Hexakis adduct of C60 with Bis(ethoxycarbonyl)methylene. *J. Am. Chem. Soc.* **1994,** *116*, 9385-9386.

TOC

Diels-Alder reaction

Orthogonal regioselectivity
by supramolecular mask-
controlled induced fit

90°
***e,e*-bis-anthracene-C$_{60}$**
(single isomer)

180°
***trans*-1-bis-pentacene-C$_{60}$**
(major product)

Supramolecular mask strategy with tetragonal prismatic nanocapsules for regiolective Diels-Alder cycloaddition using acenes is presented. A dramatic change on the host-guest interactions and equilibrium established between the firstly formed acene monoadducts induced by the length of the acene allows for the orthogonal regioselective synthesis of *e,e*-bis-anthracene-C$_{60}$ or *trans*-1-bis-pentacene-C$_{60}$ bis-adducts. The supramolecular masks strategy also allows the regioselective synthesis of equatorial tris-heterofunctionalized-C$_{60}$ adducts combining Diels-Alder with Bingel cyclopropanations. The combination of Molecular Dynamics (MD) simulations and Frontier Molecular Orbital (FMO) analyses afford a clear understanding of the regioselective control exerted by the supramolecular mask.